Proceedings of ICFDP7:
Seventh International Conference Of Fluid Dynamics And Propulsion
Dec. 19-21, 2001, Sharm El-sheik, EGYPT

THE EFFECTS OF SYSTEM ROTATION WITH THREE ORTHOGONAL ROTATING AXES ON TURBULENT CHANNEL FLOW

Osama A. El-Samni
Department of Mechanical Engineering
The University of Tokyo
Hongo 7-3-1, Bunkyo-ku
Tokyo 113-8656, Japan
Tel.: 03-5841-6419, Fax: 03-5800-6999
e-mail: elsamni@thtlab.t.u-tokyo.ac.jp

Nobuhide Kasagi
Department of Mechanical Engineering
The University of Tokyo
Hongo 7-3-1, Bunkyo-ku
Tokyo 113-8656, Japan
Tel.: 03-5841-6417, Fax: 03-5800-6999
e-mail: kasagi@thtlab.t.u-tokyo.ac.jp

Keywords: System rotation, turbulent channel flow, DNS, Coriolis effect.

ABSTRACT

The effect of Coriolis force on turbulent channel flow has been sought in a more general manner by taking into account the alignment between the rotation axis and the direction of mean pressure gradient and the rotation rate as well. Three different, but orthogonal rotation vectors coincident with the Cartesian coordinates have been imposed on a plane channel, in which homogeneity is presumed in the planes parallel to the wall. A series of DNS has been performed for each case starting from the non-rotating plane channel, while increasing the rotation number and keeping the Reynolds number based on the friction velocity at 150. Detailed statistics are obtained including mean quantities, turbulent intensities, vorticities, and higher-order moments. The budgets of transport equations of the quantities relevant to turbulence modeling are prepared for the three orthogonal cases in order to help assessing turbulence models. An attempt to investigate the near-wall structures has been tried.

INTRODUCTION

Turbulent rotating flows are of great practical importance in nature and in many industrial applications. In rotating machinery, such as pumps, compressors and gas turbines, great efforts have been directed towards exploring the transport phenomena inside the rotating passages in order to improve their performance. Coriolis and centrifugal forces affect fluid dynamics inside such rotating devices. The alignment of those body forces with respect to the bounded walls is believed to have a significant role in modifying flow structures. Various geometrical configurations are likely to exist in rotating machineries such as: rectangular ducts, pipes, U-bends, elbows, curved channels, etc., which make the flow more complicated due to the combined effect with Coriolis forces arisen from system rotation. Thus, a plane channel has been chosen in the present study in order to isolate the sole effect of Coriolis force. Moreover, the simplicity of plane channel computed with spectral methods enables changing the flow parameters, especially Reynolds and rotation numbers, and also the orientation of the rotation vector much easier than corresponding experimental setups.

Turbulent channel flow subjected to system rotation has been studied experimentally and numerically for three decades since the experimental work of Johnston et al. [1], who observed the stabilization of turbulent flow near the leading (suction) wall and the augmentation of turbulence near the trailing (pressure) wall in a spanwise rotating channel. Kim [2] used LES to study the effect of spanwise rotation and reproduced most of the observations in the experiments. Kristoffersen and Andersson [3] used DNS to study the effect of spanwise rotation using a finite difference algorithm with the rotation number, based on the friction velocity, up to 7.6 and their detailed turbulence statistics were reported by Andersson and Kristoffersen [4]. Recently, Oberlack et al. [5] studied streamwise system rotation using DNS, LES and turbulence models. The rotation numbers of 3.2 and 10 were tested in their simulations for the purpose of verifying the similarity theory. Detailed information about the flow structures have not been addressed. The present study aims at exploring the general effect of system rotation on wall-bounded flows by testing three orthogonal cases independently. The rotation number has been increased to include the ranges deduced from the conceptual design of small-scale gas turbine. Emphasis is laid upon comparing statistics, budgets and flow structures in different orientations and also with their values in non-rotating channel.

NOMENCLATURE

a_1	structure parameter
C_f	friction coefficient, $C_f = 2\tau_w / \rho U_b^2$
D_k	viscous diffusion of k
F	flatness factor
k	turbulent kinetic energy
P_k	mean production of k
Re_τ	Reynolds number, $Re_\tau = u_\tau \delta / \nu$
Ro_τ	Rotation number, $Ro_\tau = 2\delta\Omega / u_\tau$
S	skewness factor
S_{ij}	symmetric part of the strain rate tensor $(u_{i,j} + u_{j,i})/2$
T_k	turbulent transport rate of k
U, W	mean velocities in x-and z-directions
U_b	bulk velocity
u, v, w	fluctuating velocities in x-, y- and z-directions
u_τ	friction velocity
u_τ^*	friction velocity based on the total shear at both walls
x, y, z	streamwise, wall-normal and spanwise directions

Greek symbols and superscripts

δ	channel half width
γ_m, γ_g	Mean flow and gradient angles
ε_k	dissipation rate of k
Π_k	pressure diffusion of k
$-\lambda_2$	second largest eigenvalue of the tensor $S_{ik}S_{kj} + \Omega_{ik}\Omega_{kj}$
ν	kinematic viscosity
τ_w	wall shear stress
τ_w^*	modified wall shear stress in Case WN
Ω	angular velocity of system rotation
Ω_{ij}	Anti-symmetric part of strain rate tensor
ω_i	vorticity component in i^{th}–direction
+	normalized by local friction velocity u_τ and ν
*	normalized by friction velocity u_τ^* and ν

COMPUTATIONAL DETAILS

Three different cases, each of which corresponds to a different rotation vector, are tested. Cases SP, ST and WN correspond to the rotation around the spanwise, streamwise and wall-normal axes, respectively. A sketch of the computational domain is shown in Fig. 1. The rotation number $Ro_\tau = 2\Omega\delta / u_\tau$ has been increased up to 15 in Cases SP & ST. In Case WN, the maximum rotation number studied is 0.04. Five intermediate rotation cases of Ro_τ = 2.5, 5, 7.5, 11 and 15 were studied in Cases SP & ST, while only three intermediate rotation numbers of 0.01, 0.02 and 0.04 were preformed in Case WN. These ranges cover real conditions deduced from a conceptual design of small gas turbines of 30-100 kW [6]. A fully developed flow is established with periodic boundary conditions in the streamwise and spanwise directions. The driving pressure gradient is adjusted to keep the mass flow rate always constant in all simulation, and the bulk Reynolds number, $U_b\delta/\nu$, remains at 2265. The computations in each orthogonal case have been started from the initial data of non-rotating channel using coarse grids of $64 \times 65 \times 64$ in the x-, y-, and z-directions, respectively. Such coarse-grid computations help in providing the common features of low-order statistics, which are affected by system rotation.

Higher-order statistics and the budgets of the transport equations are generated for only the highest rotation numbers in each case using finer grids of 192×129×128 in Cases SP & ST and of 192×129×128 in Case WN. The computational domain has lengths of $5\pi\delta \times 2\delta \times 2\pi\delta$ in the x-, y-, and z-directions, respectively. The variables have been non-dimensionalized by the channel half width δ, friction velocity u_τ. The time step in fine grid simulations is in range of 0.045 - 0.06 u_τ^2 / ν to keep the Courant number less than 0.3 in all studied cases. Further details about the numerical techniques and the sampling procedures are referred to El-Samni [7].

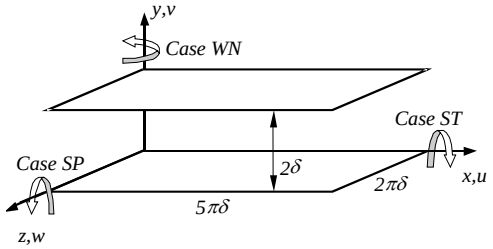

Figure 1 computational domain of rotating channel

MEAN VELOCITIES

In Case SP, asymmetric profiles of the mean velocity in the x-direction with linear slope of twice the rotation speed in the central region of the channel are recaptured well in the coarse-grid simulations. Figure 2(a) shows comparison of the present and the previous results. However, the linear profile is slightly distorted at the highest rotation number (Ro_τ = 15) giving a slope lower than twice the rotation speed and shorter width of the linear profile, which indicates a tendency to laminarizing the flow. The boundary layer thickens near the suction side (denoted by S. S. at y/δ = 1) and the velocity near the pressure side (denoted by P. S.) is largely decreased.

In Cases SP & ST, no significant change but a little flattening of U profiles appears in both cases. Noticeable shoulders are observed in Case ST as shown in Fig. 2(b). In these two cases, the mean velocity in z-direction is induced due to the non-zero Coriolis force in that direction. The induced profiles are greatly different in each case. Four zones of opposite motions have been observed in Case ST with anti-symmetric profiles around the channel centerline. The coarse-grid simulation shown in Fig 3(a) depicts this trend. The corresponding profiles in Case WN are shown in Fig. 3(b), but

the profiles are similar to that of the fully developed two-dimensional channel flow. The magnitude of this velocity component increases with increasing Ro_τ and the flow direction is then tilted in *z*-direction. Due to the induced velocity in the *z*-direction in Cases ST & WN, the flow has three-dimensional characteristics, which is more pronounced in Case ST due to the skewed profiles. The mean flow angle $\gamma_m = \tan^{-1} W/U$ and the mean gradient angle $\gamma_g = \tan^{-1}(dW/dy/dU/dy)$ differ in Case ST and change their signs more drastically, while they have closer values in Case WN (El-Samni [7]). This implies that the flow in Case WN is closer to a 2-D turbulent channel flow. A measure of flow three-dimensionality is the structure parameter a_1 defined by the ratio of the vector magnitude of the shear stress to twice the turbulent kinetic energy, which is approximately constant at 0.15 in a 2DTBL. Figure 5 shows typical profiles of a_1 in Cases ST & WN at the highest Ro_τ, where a significant distortion of a_1 in Case ST can be recognized. In Case WN, a_1 is much similar to a plane channel flow. This fact implies the two-dimensionality of the channel flow rotating around the wall-normal axis if one considers the mean flow direction as if it is tilted to the *z*-direction with an angle of γ_m.

The friction coefficients normalized by the value of non-rotating channel are presented in Fig. 5 using the results of coarse-grid computations along with the values deduced from fine-grid simulation, which is denoted by dotted symbols at only the highest Ro_τ in each case. Among the three studied cases, Case SP has distinguished behaviors at each wall. While continuous suppression of the friction coefficient takes place on the S. S. wall, the value on the P. S. wall shows non-monotonic behavior giving a peak near $Ro_\tau \approx 7.5$, beyond which continuous decrease appears indicating that increasing the rotation may lead to suppression of turbulence within the whole channel in this particular case. On the other hand the normalized C_f in Cases ST & WN increases with increasing rotation in accordance with the velocity gradient observed in Fig. 2. It is noted from Fig. 5 that Case WN exhibits comparable value of C_f to that of Case ST although the rotation number is much lower. If the integral of the Coriolis term in the *x*-momentum equation is considered in the definition of τ_w, a larger value of normalized C_f is obtained in Case WN as shown in Fig. 5.

TURBULENT INTENSITIES

The normal stresses normalized by u_τ^* in each rotation case are plotted along with those of non-rotating channel flow in Fig. 6. The '*' has been omitted for clarity. The profiles of normal stresses at a low Ro_τ of 2.5 [7] have been appended to trace the changes with the rotation number in Case SP. Much suppression at the suction side can be observed in all normal components. On the pressure side uu at low Ro_τ reveals much suppression if compared with the augmentation in the other two components vv and ww. It should be noted that vv exceeds uu in the central region of the channel in Case SP.

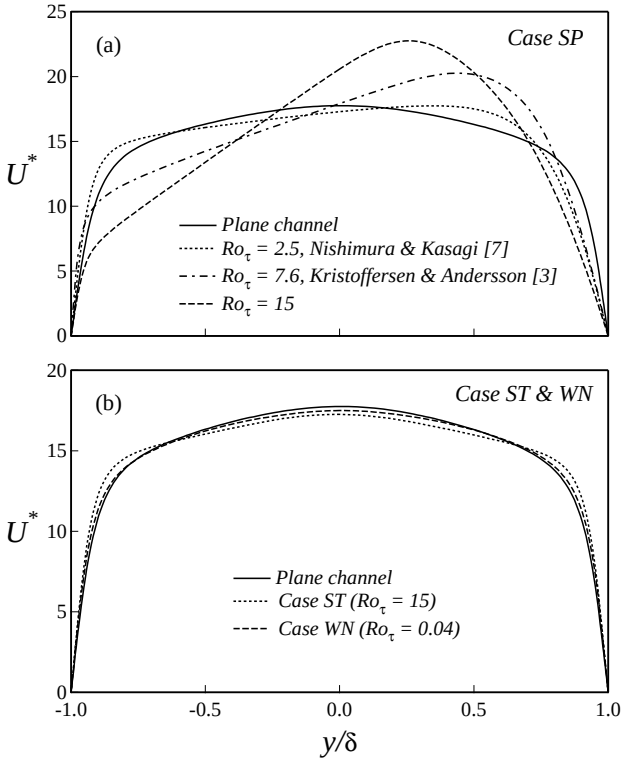

Figure 2 Mean velocity in *x*-direction; (a) Case SP; and (b) Case ST & WN.

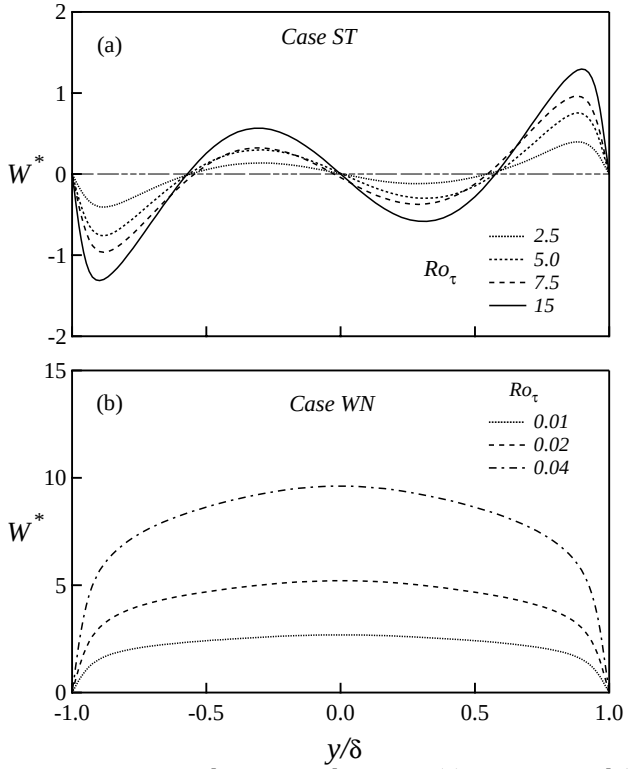

Figure 3 Mean velocity in *z*-direction; (a) Case ST; and (b) Case WN.

In Case ST $\overline{uu}$ shows slight decrement than that of non-rotating channel near the walls associated with significant augmentation of vv and ww as shown in Fig. 6. Since no rotational production term for uu, this behavior can be attributed to the role the pressure-strain correlation plays in redistributing energy from u to v and w components. In Case WN, all the normal stresses reveal augmentation especially vv and ww, although the former has no rotational production term. In Fig. 6(c), ww shows a abrupt peak, which is shifted towards the wall and similar to that of uu.

The Reynolds shear stress uv in all the studied orientations is plotted in Fig. 7, where the value of Ro_τ of 2.5 [7] is also appended. The non-monotonic behavior of normal stresses at either wall in Case ST is also observed in the trend of shear stress uv. Nearly zero values near the suction side can be observed at the Ro_τ = 15. It should be noted that the profiles of uv reveal enhancement and shifting of the linear profile down at low-to-moderate Ro_τ before they tend to decrease again beyond $Ro_\tau \sim$ 5. This behavior was well addressed in [3] and can be attributed to the sign inversion of rotational production term in the transport equation of uv, which is a function of uu - vv. It can be seen from Fig. 6 that the rotational production term at low and higher rotation numbers is negative at wide depth of the channel, which tend to reduce uv. The sign remains positive in the vicinity of the P. S., which in turn shifts the peak of $\overline{uv}$ towards the wall.

In Cases ST & WN, uv is larger than the non-rotating case, which is attributed to the direct effect of the induced rotational production terms [7]. The off-diagonal components uw and vw are non-zeros in Cases ST & WN as shown in Fig. 8. Two additional equations for the two stresses are required when dealing with second moment closures. It is worth mentioning that budgets of the transport equations for uw and vw are studied by El-Samni [7], who finds that the rotational production terms are a key role in generating such stresses in Case ST. Such budgets would be of great help to improve current turbulence models, which fail to predict the off-diagonal stresses in the study of Oberlack et al. [5]. In Case WN, although, the rotational production terms are negligible due to the weak rotation numbers imposed in this case, uw and vw profiles look like uu and uv of regular channel flow. The same similarity was observed in the budgets terms of both stresses. This suggests that Case WN can be regarded as a 2D channel flow with some tilting angle in the z-direction.

RMS VORTICITY

The dynamics of the vorticity have been addresses in the present study under the effect of different orientations by tracing the RMSs of vorticity fluctuations and their budgets, El-Samni [7]. Presented here is the RMS of ω_x shown in Fig. 9 and compared with regular channel data. Two peaks can be observed: one at the wall as a result of the opposite signed ω_x underneath the quasi-streamwise vortices and the other peak in the buffer layer due to the vortices. Although, the twp peaks exist in regular channel, their values and locations change from rotating case to another. In Case SP near the pressure side, the two peak are quite larger than regular channel flow, and the one in the buffer layer is shifted further from the wall suggesting larger diameters of the vortices. The various shapes of RMSs of ω_x in Fig. 9 imply the existence of near-wall quasi-streamwise vortices of different sizes in near-wall region.

HIGHER-ORDER STATISTICS

The skewness and flatness factors are computed for the different variables. Presented here in Fig. 10 (a), the skewness factor for the fluctuating velocity v at different orientations. For Case WN, the skewness profiles are almost the same indicating the proximity of Case WN to 2D regular channel. In Case SP, the negative skewness near the vicinity of the wall is a natural sequence of the direct effect of Coriolis force to push fluid particles towards the wall. In Case ST, the strong excursions of positive v departing from the wall towards the channel centerline and usually penetrating to the other wall are responsible for the positive skewness factor. The flatness factor on the other hand, shows higher values near the wall in all cases except Case SP.

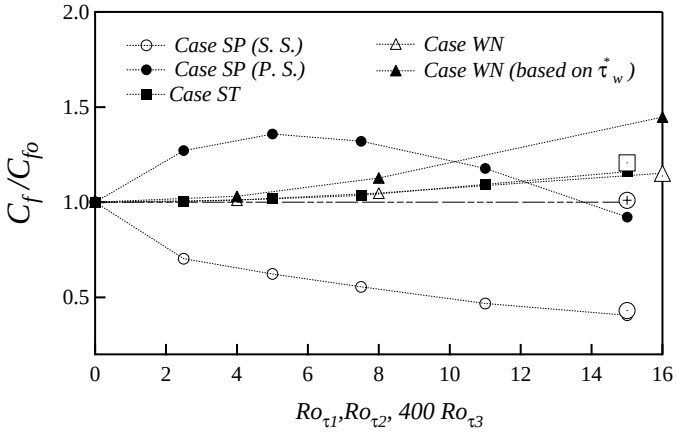

Figure 5 Normalized skin friction.

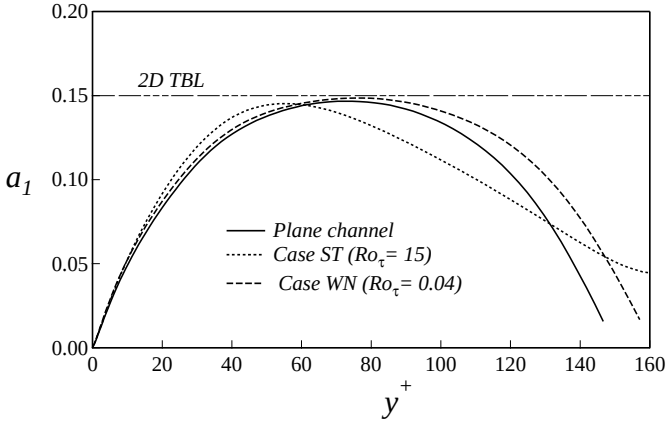

Figure 4 Structure parameter a_1 in Cases ST & WN.

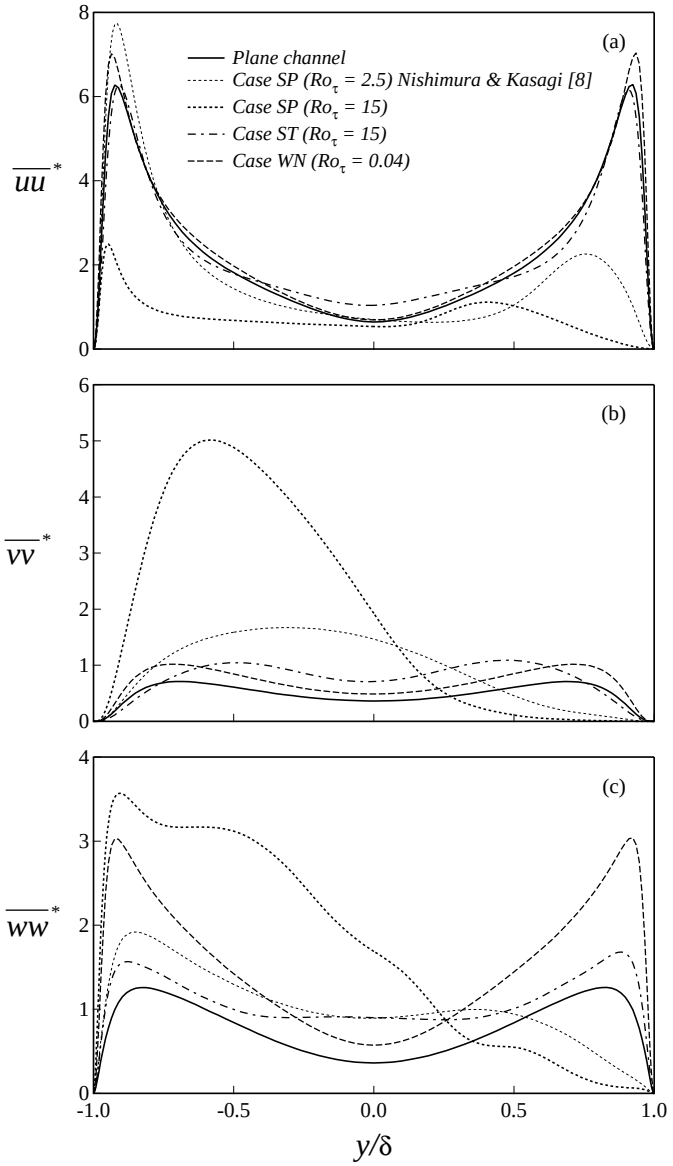

Figure 6 Normal stress in wall units; (a) uu ; (b) vv and (c) ww .

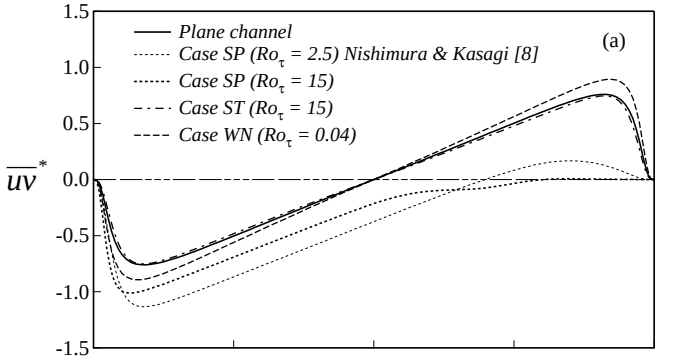

Figure 7 Reynolds shear stress uv .

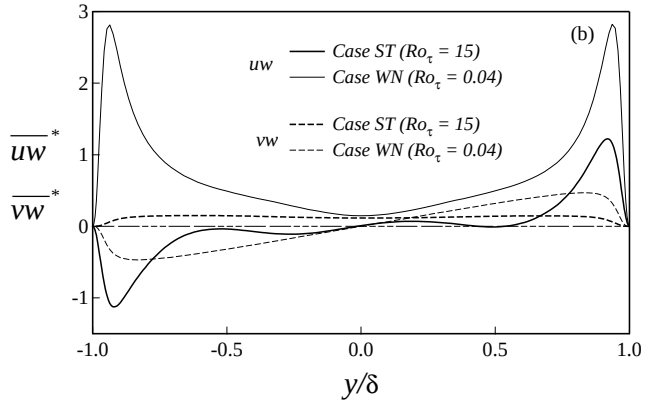

Figure 8 Off-diagonal components uw and vw .

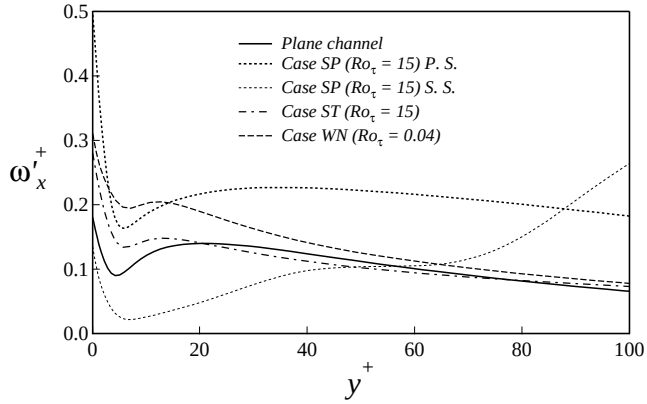

Figure 9 RMS Vorticities normalized in wall unit.

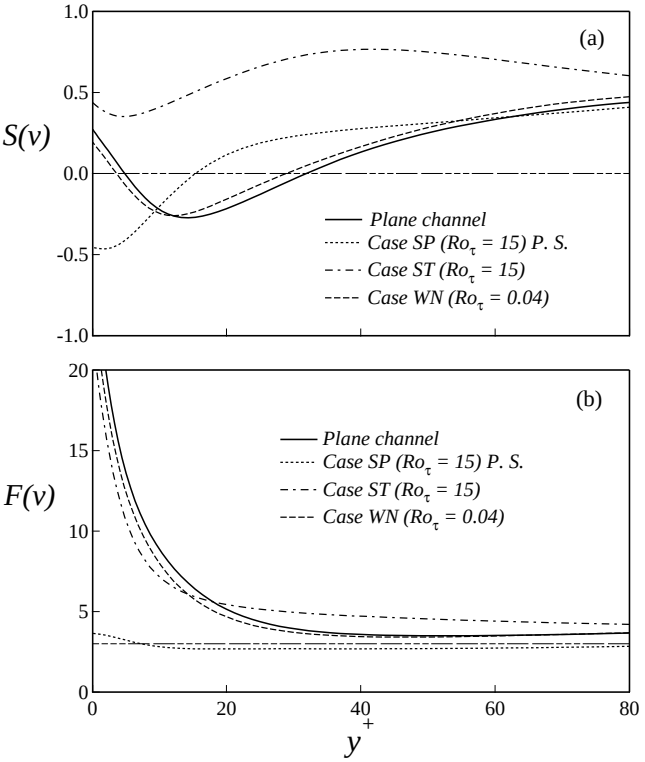

Figure 10 Skewness (a) and flatness (b) factors of v .

BUDGETS

All terms in the transport equations of the relevant quantities to turbulence models have been calculated for the different orientations studied. All components of Reynolds stresses, vorticity fluctuations, turbulent kinetic energy, and the dissipation rate of turbulent kinetic energy are of typical quantities beside other scalar related quantities. An example of the budgets computed in the present study, is the turbulent kinetic energy normalized by the wall units, which has no explicit dependence on the rotation number. However, Fig. 11 shows four different budgets of the three orthogonal orientations and the non-rotating case as well. It can be seen the drastical changes in the different terms in the budgets compared with the non-rotating case, especially in Case SP, while the general trend in Cases ST & WN seems similar to the regular channel but with a slight scaling.

TURBULENT STRUCTURES

Flow visualization for the instantaneous fields is essential tool in discovering turbulent structures in wall-bounded flows when subjected to additional strains or body forces. Cross-stream vectors can give clearer picture about the vortical structures and large scale eddies as it can be shown in Fig. 12. Two instantaneous fields in Cases SP & 2 are picked up shown the velocity vectors in *z-y* planes. It should be mentioned that Kristoffersen and Andersson [3] in Case SP at low Ro_τ observed large scale eddies of Taylor-Gortler types. However, with increasing Ro_τ the persistence of the roll cells and their sizes decreases. In Fig. 12 (a), at Ro_τ = 15, such roll cells disappear. Note that the top edge of Fig. 12(a) corresponds to the pressure side. Calm region of laminar nature can be observed in the bottom edge of this figure. In Case ST different sizes of eddy motions can be observed in Fig. 12 (b) which has rotation sign similar to the back ground rotation. Note that the flow out of the page in both graphs. The fluid particles have opposite motion at both walls, resulting in the anti-symmetric profiles shown in Fig. 3(a).

For capturing the vortical structure in rotating channel flows, the negative second largest eigenvalue (λ_2) of the tensor $S_{ik}S_{kj} + \Omega_{ik}\Omega_{kj}$ used by Jeong et al. in plane channel flow [9] which would be frame invariant and the most suitable candidate to capture vortical structures. RMS values of λ_2 are shown in Fig. 13, from which the threshold values in the visualizations are deduced. In Fig. 14, the vortical structures in three cases are embedded with the low-high speed streaks. Tilted streaks can be observed in Cases ST & WN. Less population of vortices in Case 2 is also shown; while the flow is tilted in the z-direction with more complicated structures can be shown in Fig. 14(c).

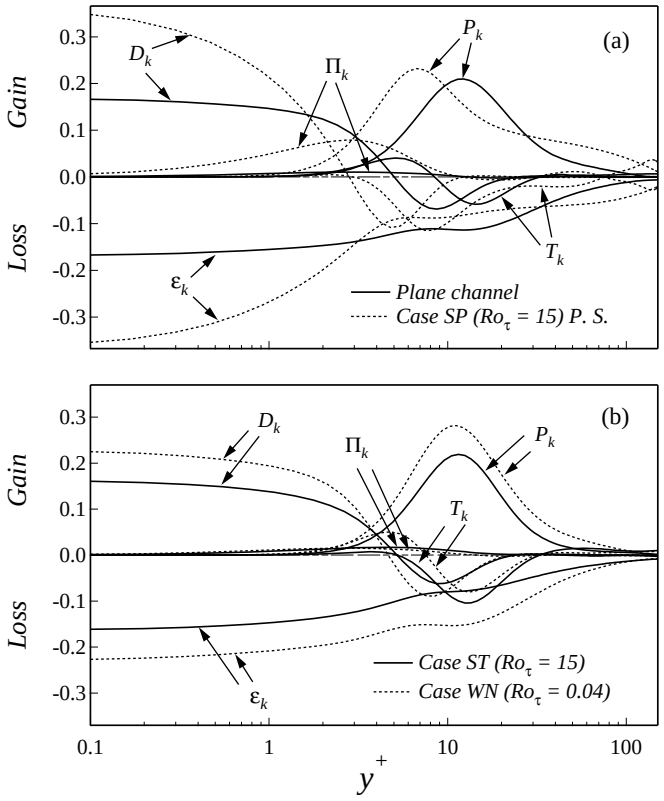

Figure 11 Terms in transport equation of turbulent kinetic energy: (a) non-rotating channel & Case SP and (b) Cases ST & WN.

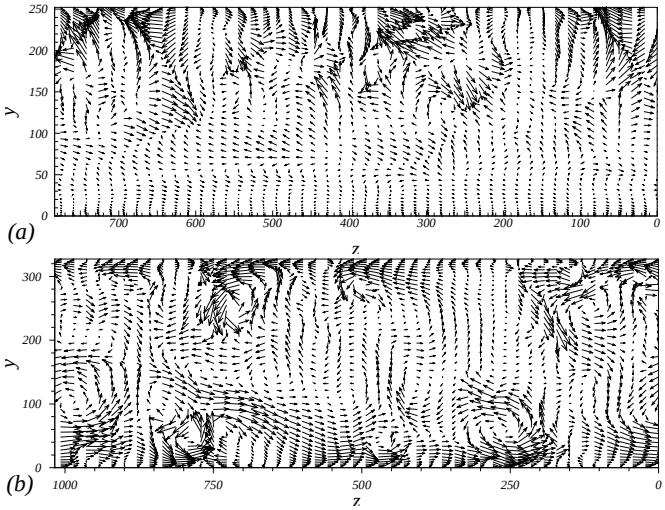

Figure 12 Cross-streamwise instantaneous velocity vector in: (a) Case SP and (b) Case ST, at Ro_τ = 15.

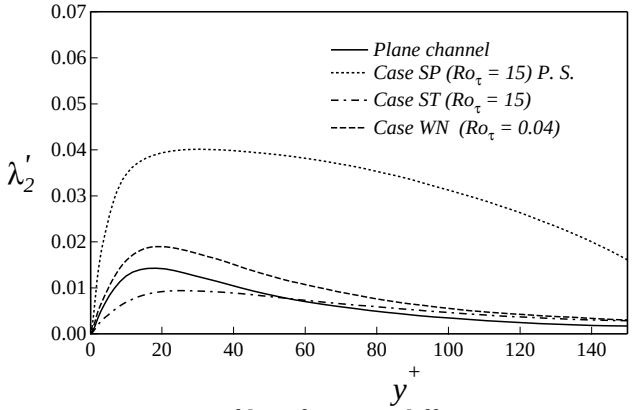

Figure 13 RMS profiles of $-\lambda_2$ in different rotating cases.

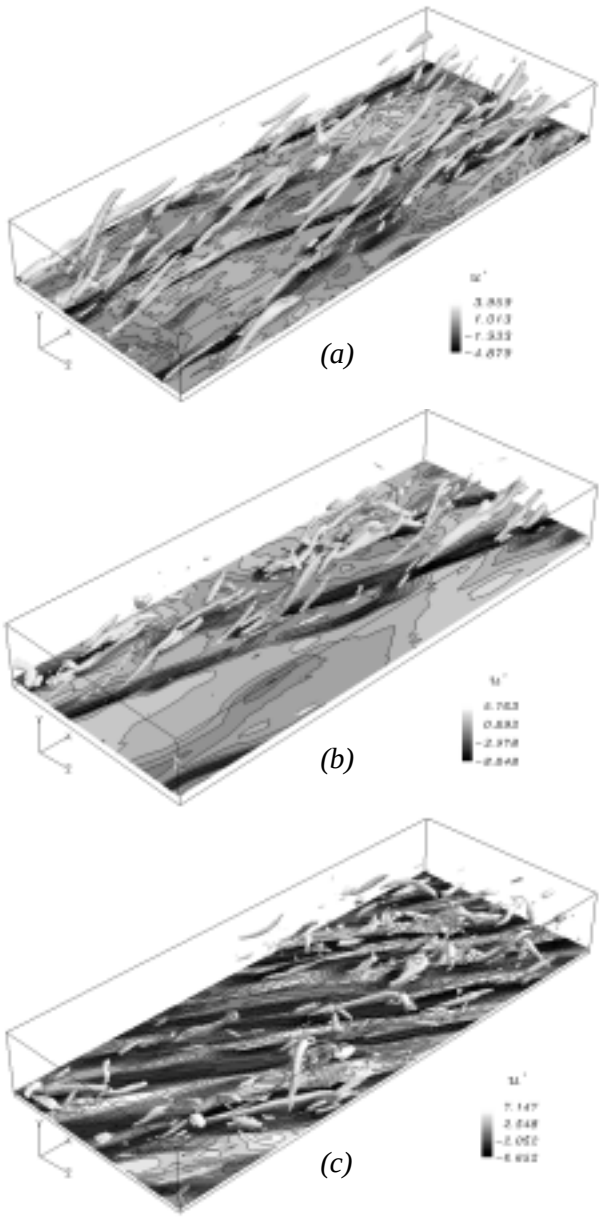

Figure 14 Vortical structures identified by $-\lambda_2$ embedded with the streaky structures in near wall region: (a) Case SP, $-\lambda_2$ = 0.056; (b) Case ST, $-\lambda_2$ = 0.02; and (c) Case WN, $-\lambda_2$ = 0.03.

CONCLUSIONS

System rotation has direct and indirect roles in modifying wall-bounded flows. Laminarization in rotating channels takes place only near the leading side in Case SP. Increasing the rotation rates may lead to laminarizing the whole flow. The linear profiles of the mean streamwise velocity are recaptured in Case SP for all the range of the rotation number, but with slight distortion at higher Ro_τ. Cases ST & WN exhibit more complicated flows. Three-dimensional flow characteristics can be deduced through the induced mean spanwise velocity and the generation of all Reynolds stress tensor components in both cases. It is shown that system rotation, when the system vorticity is perpendicular to mean flow vorticity, affects the mechanism of generating and sustaining the vortical structures near the wall of a rotating channel. Those effects are evident in Cases ST & WN, where the tilting streaky structures and less population of the vortical structures are observed. Case WN seems to be the most sensitive among the cases studied, since it produces a comparable augmentation of turbulence at a rotation number two order of magnitude smaller than those of Cases SP & ST. Databases for turbulence quantities and transport equations are generated and will be of help to assess turbulence models incorporating rotational effects.

ACKNOWLEDGMENTS

This numerical work is the results of "Micro Gas Turbine/Fuel Cell Hybrid-Type Distributed Energy System" which is supported by the Department of Core Research for Evolutional Science and Technology (CREST) of the Ministry of Education, Culture, Sports, Science and Technology (MEXT).

REFERENCES

[1] Johnson, J. P., Halleen, R. M. and Lezius, D. K., 1972, "Effects of Spanwise Rotation on The Structure of Two-Dimensional Fully Developed Turbulent Channel Flow," *J. Fluid Mech.*, **56**, pp. 533-557.

[2] Kim, J., 1983, "The Effect of Rotation on Turbulence Structure," *In Proc. of 4th Symp. on Turbulent Shear Flows*, Karlsruhe pp. 6.14-6.19.

[3] Kristoffersen, R. and Andersson, H. I., 1993, "Direct Simulations Of Low Reynolds-Number Turbulent Flow in a Rotating Channel," *J. Fluid Mech.*, **256**, pp. 163-197.

[4] Andersson, H. I. and Kristoffersen, R., 1995, "Turbulence Statistics of Rotating Channel Flow," *In the Proc. of 9th Symp. on Turbulent Shear Flows*, Kyoto, Japan, pp. 53-70.

[5] Oberlack, M., Cabot, W. & Rogers, M. M., 1999, "Turbulent Channel Flow with Streamwise Rotation: Lie Group Analysis, DNS and Modelling," *In the 1st int. Symp. in Turbulence and Shear Flow Phenomena*, USA, pp. 85-90.

[6] Fukunaga, S., 2000, "Conceptual Design of Highly Efficient Micro-Gas Turbine," Graduation thesis. (In Japanese) The University of Tokyo.

[7] El-Samni, O., 2001, "Heat and Momentum Transfer in Turbulent Rotating Channel Flow," Ph. D. thesis. The University of Tokyo, Tokyo, Japan.

[8] Nishimura, M. and Kasagi, N., 1996, "Direct Numerical Simulation of Combined and Natural Turbulent Convection in a Rotating Plane Channel," *Proc. of 3rd KSME-JSME, Thermal Engineering Conference*, Korea, Vol. 3, pp. 77-82.

[9] Jeong, J., Hussain, F., Schoppa, W. & Kim, J., 1997, " Coherent structures near the wall in a turbulent channel flow," *J. Fluid Mech.* **332**, pp.185-214.